Polar Fluorenes and Spirobifluorenes: Fluorescence and Fluorescence Anisotropy Spectra

*Luca Grisanti,† Francesca Terenziani,† Cristina Sissa,† Marco Cavazzini,‡ Fabio Rizzo,‡ Simonetta Orlandi,‡ Anna Painelli†**

† Dipartimento di Chimica GIAF and INSTM-UdR Parma, Parco Area delle Scienze 17/a, 43124 Parma, Italy;

‡ Istituto di Scienze e Tecnologie Molecolari (ISTM), Consiglio Nazionale delle Ricerche (CNR), Via C. Golgi, 19 - 20133 Milano, Italy. Polo Scientifico e Tecnologico (PTS), Consiglio Nazionale delle Ricerche (CNR), via Fantoli, 16/15 - 20138 Milano, Italy.

Abstract

An extensive spectroscopic study is presented of two asymmetrically substituted fluorene dyes and of the related spiro dimers in both liquid and glassy solvents. Essential-state models are developed to accurately reproduce linear absorption and fluorescence spectra and their complex dependence on solvent polarity. The same models are exploited to quantitatively calculate fluorescence excitation and anisotropy spectra in rigid matrixes. Impressive red-edge effects observed for spiro dimers in glassy polar solvents are accurately reproduced and understood. Interchromophore interactions in the spiro dimers are very small, leading to marginal effects in absorption and fluorescence spectra, but they effectively promote energy transfer between the two chromophores, as best evidenced comparing anisotropy spectra of the substituted fluorenes and of corresponding spiro dimers dissolved in glassy solvent matrixes.

Introduction

Molecular functional materials of interest for innovative applications in molecular electronics and photonics are most often based on large π-conjugated molecules.(1) Extended π-conjugation in fact implies large polarizabilities and hyperpolarizabilities,(2) large intramolecular charge mobility, and, thanks to the possibility of forming efficient intermolecular π–π bonds, also intermolecular charge mobility.(3) Relevant systems, including small molecules, oligomers, and polymers, have basically planar structures (or at least show planar portions in their structures), and this favors aggregation phenomena. While in some cases aggregation may enhance the properties of interest of the material at hand,(4, 5) in general it represents a drawback, because it is difficult to control and strongly affects the material's properties, most often compromising its overall performance.

Spiro bridges offer the opportunity to bind together pairs of π-conjugated structures in a rigid mutual orthogonal orientation, therefore hindering aggregation.(6, 7) At the same time, the formation of the spiro bridge is expected to only marginally affect the molecular properties: spiro conjugation is in fact weak compared to π-conjugation(8-10) and the orthogonal orientation of the molecular fragments involved in the spiro bond minimizes mutual electrostatic interactions. Indeed, interesting spiro-conjugated materials have been developed for applications in light-emitting devices.(6, 11-13) On the other hand, a nontrivial role of spiro conjugation is suggested in some systems where

improved charge transport properties are observed.(14-16) Even more intriguing is the complex photophysical behavior reported for spiro-conjugated systems.(16-18)

In this work we analyze in detail the spectral properties of two asymmetrically (donor–acceptor) substituted fluorene molecules and of the corresponding spiro dimers (Scheme 1). These molecules have been recently investigated(19) in a work focused on nonlinear optical responses. Here we collect linear absorption and fluorescence spectra of the same species in several solvents, and we set up relevant essential-state models. In agreement with previous work,(19) we conclude that the interactions in this family of spiro dimers are small, leading to minor spectroscopic effects on absorption and fluorescence spectra. However, quite impressive variations of the fluorescence quantum yield suggest that the photophysics of these systems is strongly affected by the crowding of excited states in spiro dimers. More detailed and reliable information about energy transfer between the excited states of spiro dimers is obtained from fluorescence anisotropy spectra collected in glassy solutions of solvents with different polarities. The important red-edge effect observed in glassy matrixes obtained from polar solvents, quantitatively reproduced based on essential-state models, unambiguously demonstrates that interchromophore interactions, which only marginally affect absorption and fluorescence spectra, are large enough to induce efficient energy transfer between excited states of spiro dimers.

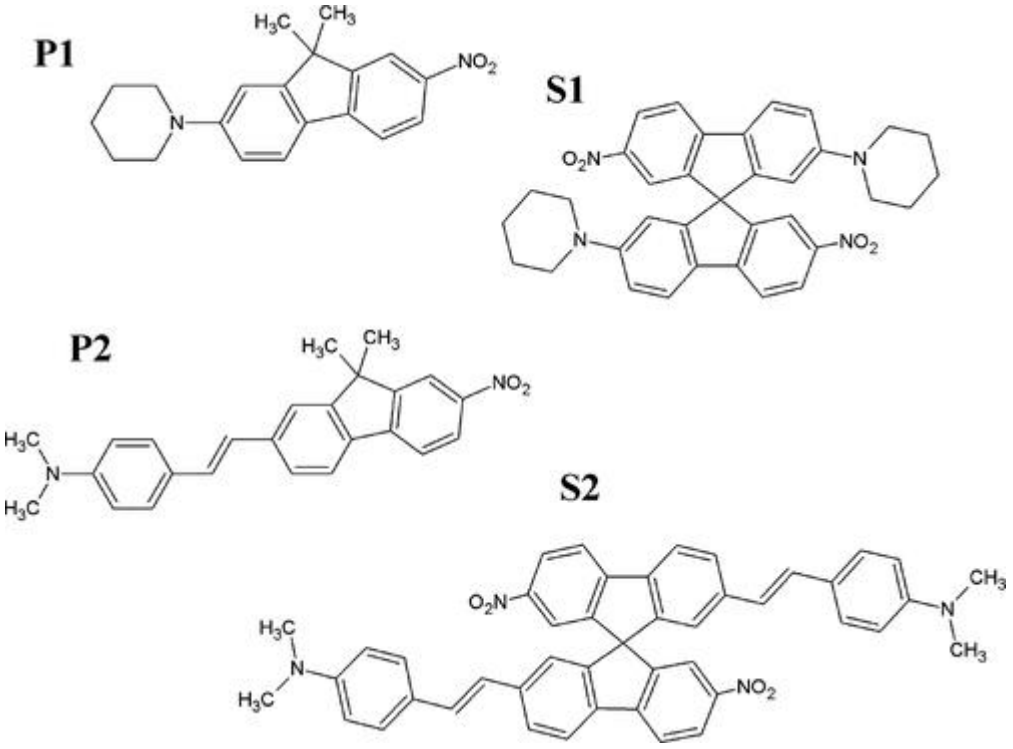

Scheme 1 Scheme 1. Molecular Structures of the Investigated Compounds[a]
a **P1** and **P2** are polar chromophores, while **S1** and **S2** are the corresponding spiro-conjugated bichromophores.

Experimental Section

Materials

The syntheses of 9,9-dimethyl-2-nitro-7-piperidin-1-ylfluorene (**P1**), (*E*)-9,9-dimethyl-2-[2-(4-*N*,*N*-dimethylaminophenyl)ethen-1-yl]-7-nitrofluorene (**P2**), 2,2′-dinitro-7,7′-dipiperidin-1-yl-9,9′-

spirobifluorene (**S1**), and (*E*,*E*)-2,2′-bis[2-(4-*N*,*N*-dimethylaminophenyl)ethen-1-yl]-7,7′-dinitro-9,9′-spirobifluorene (**S2**) have been previously reported, together with the synthetic details and chemical–physical characterization.(19)

The solvents used for spectroscopic measurements were the following: decahydronaphthalene (decalin in the following; from Sigma-Aldrich, cis + trans mixture, purum, >99.0%); toluene (Sigma-Aldrich, for HPLC, ≥99.9%); 2-methyltetrahydrofuran (2-MeTHF; Sigma-Aldrich, anhydrous, >99.0%); chloroform ($CHCl_3$; Riedel-de Haën, spectra grade). For low-temperature measurements, 2-MeTHF was used after overnight storage on molecular sieves (0.3 nm). Other solvents were used as received.

Spectroscopic Measurements

Absorption spectra were collected on a Lambda 650 UV/vis Perkin-Elmer spectrophotometer on solution of $\sim 10^{-5}$ M. Fluorescence and fluorescence excitation spectra were recorded on a Fluoromax-3 Horiba Jobin-Yvon spectrofluorometer. To minimize self-absorption processes, these measurements were run on solutions of $\sim 10^{-6}$ M. Fluorescence quantum yields (FQY) were measured in toluene by using fluorescein (0.1 M NaOH) as the standard (FQY = 90%). The spectrofluorometer was equipped with excitation and emission Glan-Thompson automatic polarizers for anisotropy measurements (single-channel L-format). Fluorescence anisotropy is defined as(20)where $I_{\parallel}$ is the emission intensity measured when the excitation and emission polarizers are parallel, while $I_{\perp}$ is the emission intensity when the two polarizers are mutually perpendicular. Anisotropy measurements were run as described in ref 24 on glassy matrixes obtained upon fast cooling of 2-MeTHF and decalin solutions. Light-scattering phenomena are not expected in glassy solutions. In any case, a spectral resolution of 1 nm was adopted in all measurements, so residual scattered light can hardly reach the detector except in the very close proximity of the excitation line. The main source of noise in anisotropy spectra is indeed related to the imposed high spectral resolution. The rotation of the solute molecules is completely hindered in frozen solutions, so anisotropy results give reliable information on the relative orientation of absorption and emission transition dipole moments. Anisotropy spectra can also be measured at room temperature in highly viscous liquids, but we prefer using frozen solutions where not only the motion of the solute but also that of the solvent molecules is blocked. As discussed in the following, this helps in setting up quantitative models for anisotropy. Moreover, more resolved spectra are obtained at low temperature.

All spectra are reported versus an inverse wavelength scale, proportional to the energy, to facilitate the visual comparison of bandwidths and band shapes of transitions occurring in different spectral regions.

Absorption, Fluorescence, and Fluorescence Anisotropy Spectra

Absorption and fluorescence spectra collected in solvents of different polarities are shown in Figure 1. Experimental data for toluene solutions are summarized in Table 1. Absorption and fluorescence spectra of **P1** and **P2** show a normal solvatochromism, suggesting a largely neutral ground state and

a charge-separated excited state. **S1** and **P1** spectra are practically superimposed, with the extinction coefficient of **S1** twice that of **P1** (cf. Table 1), suggesting negligible interactions between the two chromophoric units in the spiro dimer. Absorption and emission spectra of **S2** are slightly red-shifted (~10–15 nm) with respect to **P2** in all solvents, suggesting weak interactions between the two chromophoric units. This weak interaction barely affects the molar extinction coefficient that shows additive behavior. Fluorescence quantum yields of spiro dimers are smaller than those measured for the corresponding monomers, particularly so for the **P1**/**S1** pair (cf. Table 1), suggesting a major role of the spiro linkage in the photophysics of these systems. (16-18) Both **P2** and **S2** are poorly fluorescent in polar solvents.

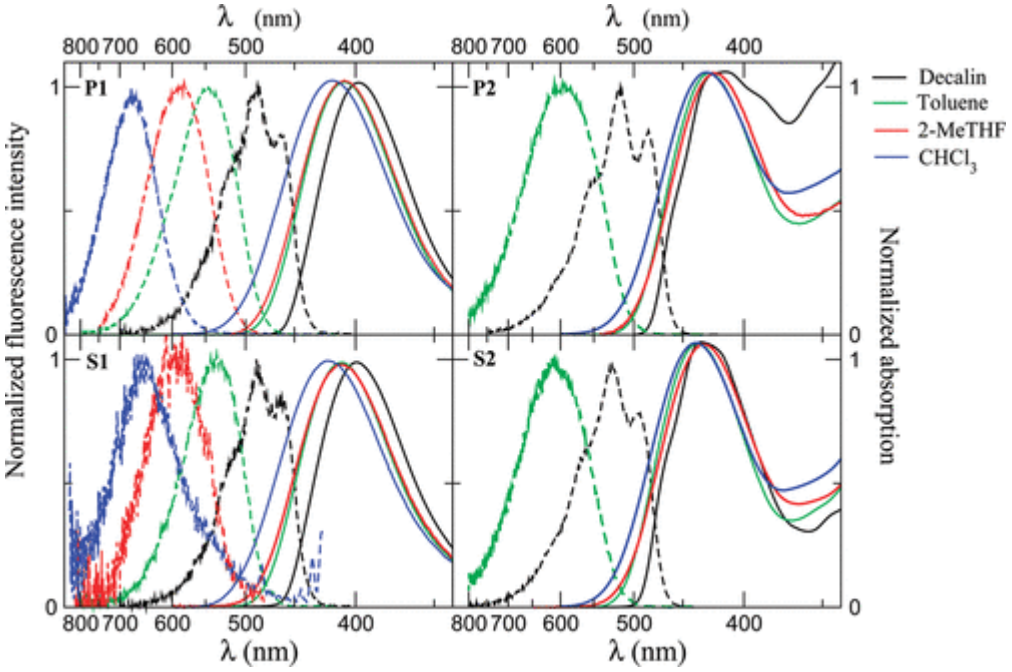

Figure 1. Top panels: absorption (continuous lines) and fluorescence (dashed lines) spectra of dipolar chromophores in solvents of different polarities (room-temperature data). Bottom panels: absorption and fluorescence spectra of the corresponding spiro dimers in the same solvents. The fluorescence signals from **P2** and **S2** in polar solvents are too weak to obtain reliable spectra.

Table 1. Experimental Spectroscopic Data of **P1**, **S1**, **P2**, and **S2** in Toluene (Room Temperature)

	λ_{abs} (nm)	λ_{em} (nm)	ε^a (M^{-1} cm^{-1})	FQY[b] (%)
P1	408	547	20 400	65
S1	411	536	39 400	9
P2	427	599	32 300	45
S2	437	612	64 600	27

[a] Molar extinction coefficient, with estimated uncertainty 5%.
[b] Fluorescence quantum yield, with estimated uncertainty 10%.

In the nonpolar solvent decalin all compounds show emission spectra with a well-resolved vibronic structure, while in the same solvent the vibronic structure of absorption spectra is blurred. Moreover, an anomalously large Stokes shift is observed for all chromophores in nonpolar solvents (decalin and toluene).

Figure 2 shows fluorescence emission and excitation spectra of all compounds in glassy decalin and 2-MeTHF solutions. Excitation spectra were collected detecting at the wavelength of maximum emission, and emission spectra were recorded exciting at the wavelength of maximum absorption. Measurements were run at 200 K in decalin and at 77 K in 2-MeTHF: at these temperatures the solvents are rigid matrixes. Under these conditions, the orientational motion of both solute and solvent molecules is precluded during the excited-state lifetime, so the solvent cannot relax after photoexcitation. Moreover, due to the reduced temperature, spectroscopic effects related to inhomogeneous broadening are reduced. Accordingly, low-temperature excitation and emission bands show a more resolved vibronic structure than the corresponding room-temperature spectra. In particular, some hint of vibronic structure is visible in the low-temperature absorption spectra in decalin. Nonradiative decay processes are hindered in rigid matrixes, favoring emissive channels so that emission is measurable also for **S2** and **P2** in the polar 2-MeTHF solvent at low temperature. Excitation spectra in 2-MeTHF are red-shifted compared to spectra at room temperature because the dielectric constant and refractive index of the solvent increase with decreasing temperature.(21) In decalin the Stokes shifts measured for all compounds are barely affected by temperature, while in 2-MeTHF the Stokes shifts decrease upon lowering the temperature, becoming comparable to those observed in decalin. This behavior is consistent with the presence of one or more low-frequency modes that, remaining unfrozen at low temperature, relax after photoexcitation.(22) We account for this residual relaxation introducing a low-frequency conformational molecular mode that, as discussed in detail below, will also explain the observation of broader absorption than fluorescence bands.(23)

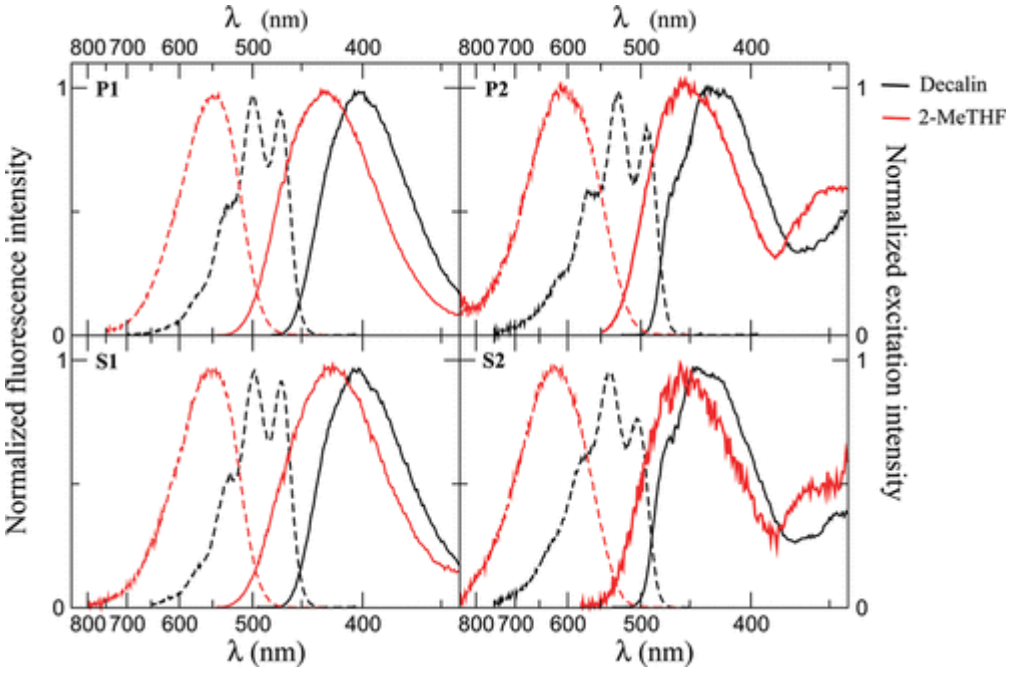

Figure 2. Top panels: fluorescence excitation (continuous lines) and emission (dashed lines) spectra of **P1** and **P2** in undercooled decalin (200 K) and glassy 2-MeTHF (77 K). Bottom panels: the same for the corresponding spiro dimers (**S1** and **S2**).

Figures 3 and 4 show spectra collected for the **P2**/**S2** pair in glassy decalin and 2-MeTHF, respectively. Spectra for the **P1**/**S1** pair, available as Supporting Information, are similar. Emission anisotropy spectra (left panels of both figures) are recorded as a function of the wavelength of emitted light upon excitation at several wavelengths (marked by arrows in the right panels). Excitation anisotropy spectra (right panels of Figures 3 and 4) are collected as a function of the excitation wavelength, measuring the intensity of the light emitted at the wavelengths marked by arrows in the left panels. Quite irrespective of the solvent, anisotropy spectra of **P2** (top panels of Figures 3 and 4) are flat, with $r > 0.3$, not far from the limiting $r = 0.4$ value expected for systems with parallel absorption and fluorescence transition dipole moments. This behavior is typical of linear donor–acceptor chromophores, in which the transition dipole moments relevant to absorption and emission processes are almost aligned along the main molecular axis.(24) Anisotropy spectra of **S2** (bottom panels of Figures 3 and 4) show a qualitatively different and solvent-dependent behavior. Excitation anisotropy spectra collected in decalin (Figure 3, bottom right panel) do not depend on the detection wavelength and show an almost constant value ($r \sim 0.1$) in the region of the excitation band, increasing toward larger values just in the far red edge of the excitation band. Accordingly, emission anisotropy spectra are flat within the emission band, and are barely affected by the excitation wavelength. Overall, emission and excitation spectra of **P2** and **S2** in undercooled decalin are marginally sensitive to excitation and detection wavelengths, respectively, and r is large (>0.3) for **P2** and small (~0.1) for **S2**.

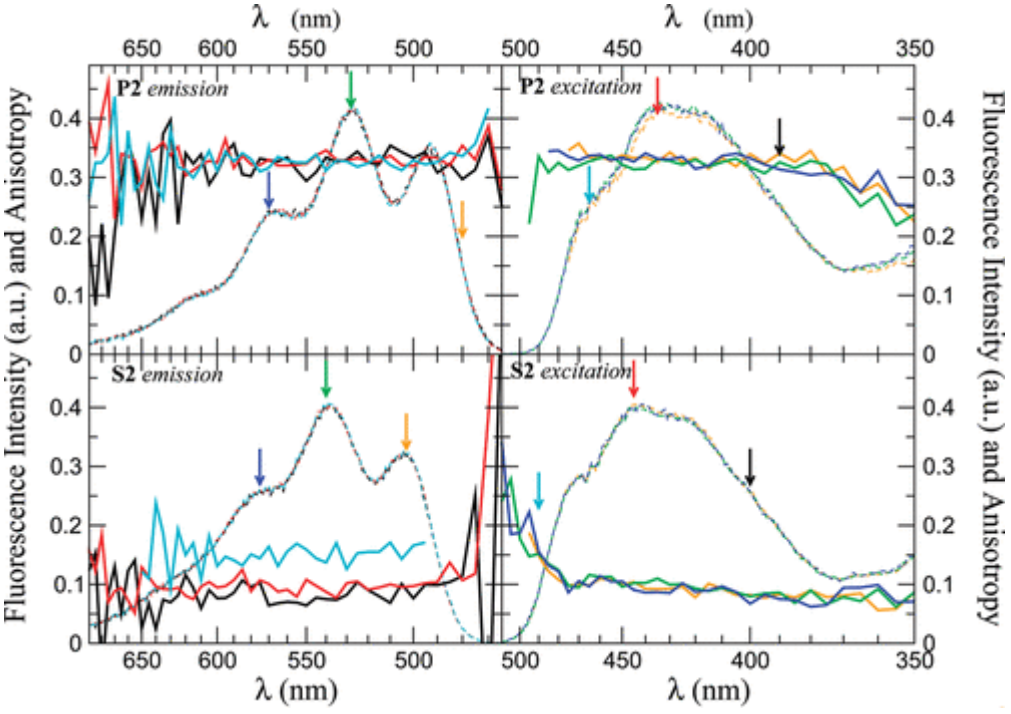

Figure 3. Fluorescence and fluorescence anisotropy spectra of **P2** (top panels) and **S2** (bottom panels) in decalin at 200 K. Thin continuous and dashed lines refer to fluorescence anisotropy and to fluorescence spectra, respectively. Bold lines refer to anisotropy spectra. Left panels: emission spectra collected exciting the sample at different wavelengths (black = 390 nm for **P2** and 400 nm for **S2**, red = 435 nm for **P2** and 445 nm for **S2**, cyan = 465 nm for **P2** and 490 nm for **S2**, as

shown by arrows in the right panels). Right panels: excitation spectra collected detecting the light at different wavelengths (orange = 480 nm for **P2** and 503 nm for **S2**, green = 528 nm for **P2** and 540 nm for **S2**, blue = 570 nm for **P2** and 575 nm for **S2**, as shown by arrows in left panels).

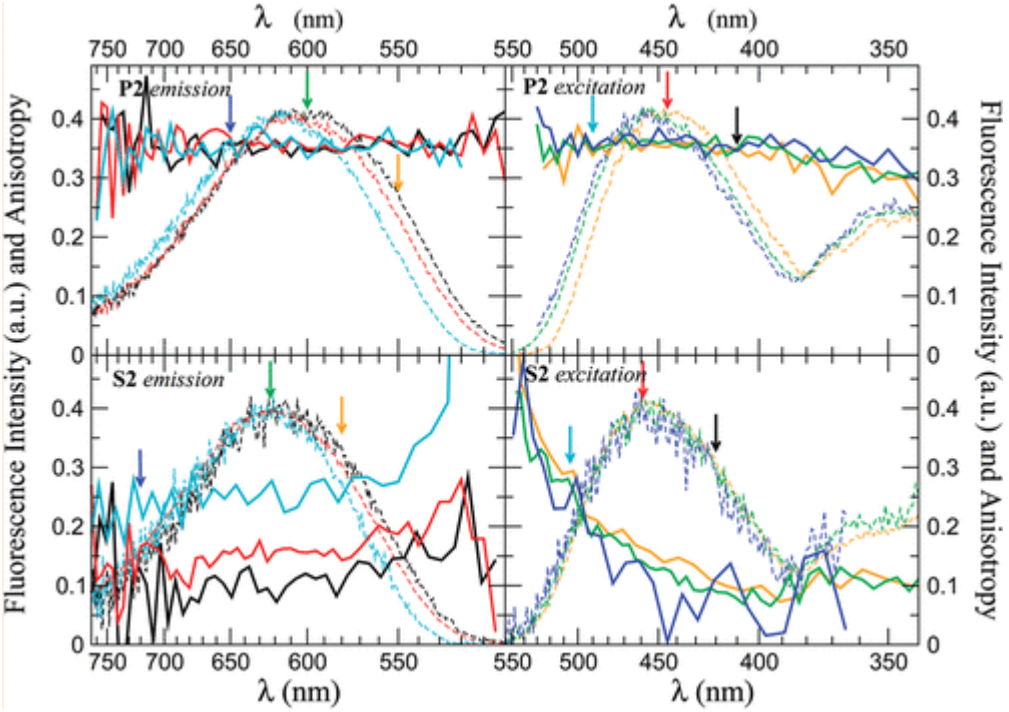

Figure 4. Fluorescence and fluorescence anisotropy spectra of **P2** (top panels) and **S2** (bottom panels) in 2-MeTHF at 77 K. Continuous lines refer to fluorescence anisotropy spectra; dashed lines refer to fluorescence spectra. Left panels: emission spectra collected exciting the sample at different wavelengths (black = 410 nm for **D2** and 420 nm for **S2**, red = 445 nm for **D2** and 458 nm for **S2**, cyan = 490 nm for **D2** and 505 nm for **S2**, as shown by arrows in the right panels). Right panels: excitation spectra collected detecting the light at different wavelengths (orange = 550 nm for **D2** and 580 nm for **S2**, green = 600 nm for **D2** and 623 nm for **S2**, blue = 650 nm for **D2** and 720 nm for **S2**, as shown by arrows in left panels).

Excitation anisotropy spectra of **S2** in 2-MeTHF (bottom right panel of Figure 4) qualitatively differ from spectra collected in decalin: they show a low *r* (~0.1) value in the blue side of the excitation band, but the anisotropy increases rapidly *within* the band, reaching the *r* = 0.4 limiting value in the red edge of the band. This result is independent of the detection wavelength. Accordingly, emission anisotropy spectra are flat within the emission band, but their values vary with the excitation wavelength: *r* is low (~0.1) for excitation in the blue side of the absorption band but rapidly increases toward the limiting 0.4 value when the excitation wavelength is moved toward the red.

Setting the Stage: Essential-States Models for Optical Spectra in Liquid Solution

Two-State Model for the Isolated Chromophores

The standard essential-state model for optical spectra of polar chromophores in solution accounts for two electronic basis states, corresponding to the two resonating structures, $|DA\rangle$ and $|D^+A^-\rangle$, separated by an energy gap 2η, and mixed by a matrix element $-\tau$.(25) The coupling between electronic and vibrational degrees of freedom is introduced, accounting for one effective vibrational coordinate *Q*, with frequency ω_v and relaxation energy ε_v.(25) Polar solvation is described by the reaction field *F*, with ε_{or} measuring the solvent relaxation energy. (23, 26) Finally, to account for the

observation of broad absorption spectra and sizable Stokes shifts in nonpolar solvents, we introduce a slow internal coordinate, *R*, related to a conformational mode that modulates the hopping integral τ with relaxation energy ε_R. (22, 27) The total Hamiltonian reads

$$H_P = 2\eta\hat{\rho} - \tau\hat{\sigma} - \sqrt{2\varepsilon_v}\omega_v Q\hat{\rho} - F\hat{\mu} - R\hat{\sigma} + \frac{1}{2}(\omega_v{}^2 Q^2 + P^2) + \frac{\mu_0{}^2}{4\varepsilon_{or}}F^2 + \frac{1}{4\varepsilon_R}R^2 \qquad (2)$$

where $\hat{\sigma} = |DA\rangle\langle D^+A^-| + |D^+A^-\rangle\langle DA|$ and $\hat{\rho} = |D^+A^-\rangle\langle D^+A^-|$. The operator $\hat{\rho}$ measures the weight of the zwitterionic state, and is therefore proportional to the charge separation. The dipole moment operator is proportional to $\hat{\rho}$, with $\hat{\mu} = \mu_0\hat{\rho}$, where $\mu_0 = \langle D^+A^-|\hat{\mu}|D^+A^-\rangle$ measures the dipole moment of the $|D^+A^-\rangle$ state.(25) The sixth term in H_P describes the harmonic oscillator associated with the internal coordinate *Q*, with *P* representing the conjugated momentum. Both *F* and *R* are associated with slow motions and will be treated as classical variables, neglecting the relevant kinetic energies. The last two terms in H_P then describe the elastic potentials associated with the two classical coordinates.

Since *F* and *R* are classical coordinates, the Hamiltonian in eq 2 becomes a function of *F* and *R*. $H_P(F,R)$ describes a coupled electronic and vibrational problem that is numerically solved without introducing additional approximations. Specifically, the (*F*- and *R*-dependent) Hamiltonian matrix can be written on the basis obtained as the direct product of the two electronic states ($|DA\rangle$ and $|D^+A^-\rangle$) times the first *M* eigenstates of the harmonic oscillator associated with *Q*. The resulting Hamiltonian matrix has dimensions $2M \times 2M$ and is diagonalized to get numerically exact nonadiabatic (*F*- and *R*-dependent) eigenstates. In this work $M = 12$ proved large enough to obtain *M*-independent results.

The nonadiabatic eigenstates resulting from the diagonalization of $H_P(F,R)$ are used to calculate absorption and emission spectra according to explicit expressions in ref 28, where a Gaussian line shape is assigned to each transition, with fixed half-width at half-maximum, Γ. The calculation is repeated on a grid of points in the *F*,*R* plane: solution spectra are finally obtained as Boltzmann averages of the contributions from the points in the grid. Specifically, absorption and fluorescence spectra in liquid solutions are calculated accounting for the Boltzmann distribution relevant to the ground state and to the fluorescent state, respectively.

Figure 5 shows calculated absorption and fluorescence spectra for **P1** and **P2**, to be compared with experimental spectra in the top panels of Figure 1. Model parameters are listed in Table 2. The two-state model reproduces very well the solvent evolution of absorption and fluorescence spectra in terms of both band position and shape. Having introduced a conformational degree of freedom, we also reproduce the anomalously large Stokes shifts observed in the nonpolar decalin solvent, as well as the observation of broad, unstructured absorption bands in the same solvent.

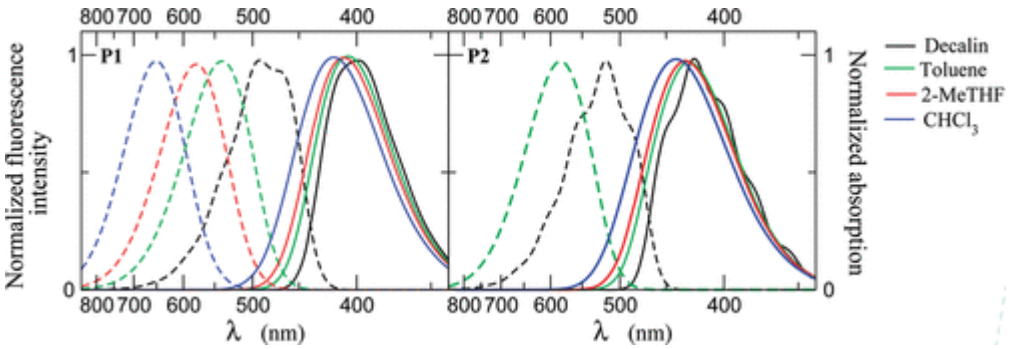

Figure 5. Room-temperature absorption and fluorescence spectra (continuous and dotted lines, respectively) calculated for **P1** and **P2** adopting model parameters listed in Table 2.

Table 2. Essential-State Molecular and Solvent Parameters for the **P1**, **S1** and **P2**, **S2** Pairs

solvent-independent molecular parameter	**P1 and S1**	**P2 and S2**
η (eV)	1.28 (1.15)a	1.27 (1.2)a
τ (eV)	0.9	0.84
μ_0 (D)	18.5	26
ε_R (eV)	0.08	0.05
ε_v (eV)	0.4	0.5
ω_v (eV)	0.19	0.17
Γ (eV)	0.05	0.04
*V*b (eV)	0	–0.4
solvent relaxation energies, ε_{or} (eV)		
decalin	0.02	0.02
toluene	0.25	0.27
2-MeTHF	0.4	0.4
chloroform	0.7	0.7

[a]Parameters adopted to reproduce spectra in glassy 2-MeTHF matrixes.
[b]Only applies to **S1** and **S2**.

Four-State Models for Spiro Dimers

Following a bottom-up approach,(5, 28-33) the model for spiro dimers is built based on the model developed for the isolated chromophores and explicitly accounting for effective electrostatic interchromophore interactions. The electronic Hamiltonian is then defined on the basis of the four

electronic states, $|DADA\rangle$, $|D^+A^-DA\rangle$, $|DAD^+A^-\rangle$, and $|D^+A^-D^+A^-\rangle$, as schematically shown in the left panel of Figure 6. On this basis we introduce the electronic operators $\hat{\rho}_1 = |D^+A^-DA\rangle\langle D^+A^-DA|$, $\hat{\rho}_2 = |DAD^+A^-\rangle\langle DAD^+A^-|$, $\hat{\sigma}_1 = |DADA\rangle\langle D^+A^-DA|$, and $\hat{\sigma}_2 = |DADA\rangle\langle DAD^+A^-|$, where the 1, 2 indices mark operators relevant to the two chromophoric units within the spiro dimer. Similarly, two vibrational coordinates, Q_1 and Q_2, and their conjugated momenta, P_1 and P_2, two internal conformational coordinates, R_1 and R_2, and two orientational reaction fields, F_1 and F_2, are introduced, where again the indices refer to the two chromophores. Since the two chromophores in a spiro dimer are equivalent, the same model parameters, η, τ, ε_v, ω_v, μ_0, ε_{or}, and ε_R, apply to the two chromophores, so that the Hamiltonian for the spiro dimer reads

$$H_S = H_{P1} + H_{P2} + V\hat{\rho}_1\hat{\rho}_2 \qquad (3)$$

where H_{P1} and H_{P2} are the Hamiltonians relevant to the two chromophores, obtained from eq 2, substituting all operators and coordinates with those relevant to chromophores 1 and 2, respectively. The last term in H_S describes an effective interchromophore interaction where V measures the interaction energy between the two zwitterionic chromophores. In the spirit of bottom-up modeling, all model parameters entering H_{P1} and H_{P2} are fixed to the values obtained from the analysis of solution spectra of the isolated chromophores, and only the effective parameter V is adjusted to reproduce optical spectra of spiro dimers. As shown in the right panel of Figure 6, the degeneracy of the two lowest-energy excitations is removed for finite V.

According to chemical intuition, and as recently confirmed by density functional theory (DFT) calculations,(19) the two chromophoric units in the spirobifluorene systems are mutually orthogonal. Fixing a coordinate system with the x- and y-axes parallel to the two chromophoric units,

the dipole moment operator of spiro dimers is defined by its components: Accordingly, the two reaction fields, F_1 and F_2, coincide with the two components of the reaction field, F_x and F_y, respectively.

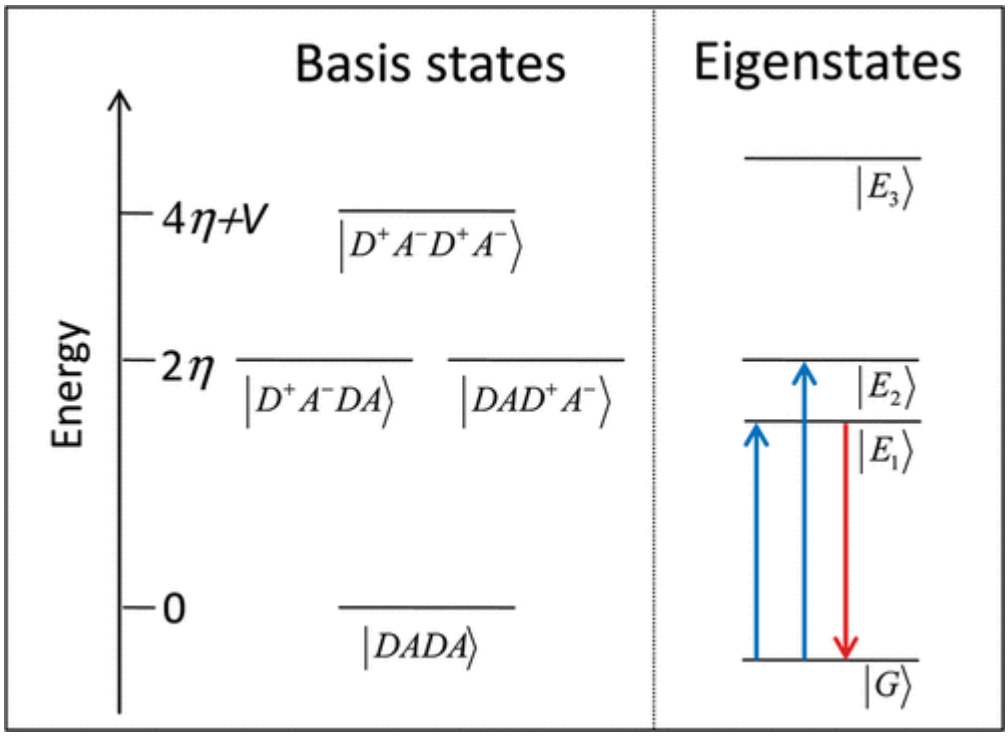

Figure 6. Schematic diagram for the electronic states of spiro dimers.

The spiro-dimer Hamiltonian in eq 3 depends on four classical coordinates F_x, F_y, R_1, and R_2. We therefore define a grid of points in the hyperspace spanned by the four coordinates, and we numerically diagonalize $H_S(F_x,F_y,R_1,R_2)$ on each point of the grid. Specifically, the Hamiltonian matrix is written on the basis obtained as the direct product of the four electronic basis states times the eigenstates of the two harmonic oscillators, Q_1 and Q_2, truncated to the lowest-energy M states. The resulting matrix of dimension $4M^2 \times 4M^2$ is diagonalized to get numerically exact eigenstates with large enough M to ensure convergence. $M = 12$ is relevant to this work.

Absorption and fluorescence spectra are calculated on each point of the grid using equations in ref 28. Spectra in liquid solutions are finally obtained as Boltzmann averages over the grid, based on the ground- and fluorescent-state energies for absorption and fluorescence spectra, respectively.

Figure 7 shows absorption and emission spectra of the spiro-conjugated chromophores calculated in solvents of different polarities at room temperature, to be compared with experimental spectra in Figure 1. Relevant model parameters are listed in Table 2. The agreement between theory and experiment is very good, particularly in view of the reduced number of model parameters. The interchromophore interaction is negligible for **S1**, and small for **S2**, if compared with other electronic energies, η and τ (cf. Table 2).

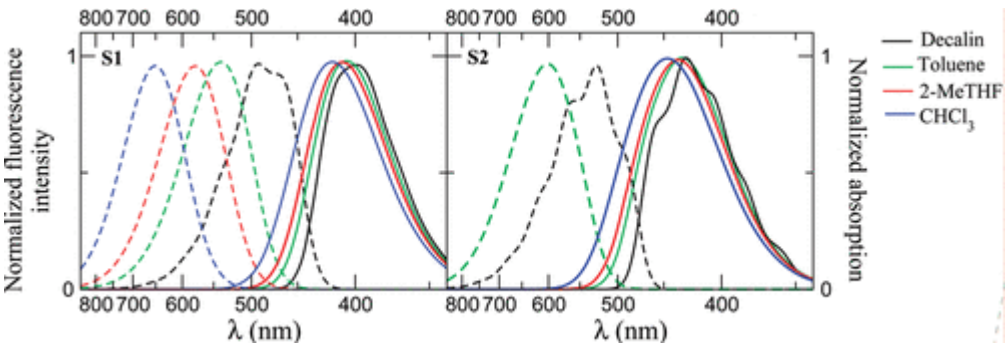

Figure 7. Room-temperature absorption and fluorescence spectra (continuous and dotted lines, respectively) calculated for **S1** and **S2** adopting model parameters listed in Table 2.

Optical Spectra in Glassy Solutions: Fluorescence Excitation and Anisotropy Spectra

Temperature explicitly enters our model through the Boltzmann distributions. However, other phenomena must be accounted for to describe spectra collected in frozen solution. The first and most important phenomenon is related to fluorescence spectra. In fact, after photoexcitation the rigid solvent matrix cannot relax in response to the variation of the charge distribution in the excited solute. Therefore, fluorescence spectra in glassy solutions must be calculated imposing the same distribution of reaction field as used for the calculation of absorption spectra. This explains the observation of smaller Stokes shifts in frozen polar solvents with respect to liquid solvents. Indeed, in the absence of any internal conformational degree of freedom, one would expect vanishing Stokes shifts in glassy solvents, quite irrespective of the solvent polarity. The second, more subtle effect is related to the temperature dependence of solvent properties, including density, refractive index, and dielectric constant. As a result, the solvent relaxation energy, ε_{or}, is in principle temperature dependent, and some variation of molecular parameters is also expected related to the variation of the solvent refractive index.(22, 26) In our analysis we try to maintain the number of adjustable parameters at a minimum, assuming in most cases temperature-independent model parameters. Exceptions to this (restrictive) rule will be explicitly mentioned.

The calculation of optical spectra, including fluorescence and fluorescence excitation anisotropy in frozen solutions, has been recently addressed for polar and octupolar dyes.(24) The extension of the analysis to spiro dimers is nontrivial due to the presence of an internal conformational mode that, at variance with the reaction field, relaxes after photoexcitation. For either the isolated chromophores or the spiro dimers, anisotropy spectra are calculated on the points of a grid in the (hyper)space defined by the slow variables associated with the reaction field(s) and conformational mode(s). For each point of the grid $I_{\parallel}$ and $I_{\perp}$, the intensities of light emitted with parallel polarization and perpendicular polarization to the excitation light, are calculated as follows:(24)

$$I_{\parallel}(\lambda_{exc}, \lambda_{em}) = \frac{1}{15}\sum_{i,j} A_i(\lambda_{exc})\, F_j(\lambda_{em})[1 + 2\, cos^2\, \theta_{ij}] \qquad (5a)$$

$$I_{\perp}(\lambda_{exc}, \lambda_{em}) = \frac{1}{15}\sum_{i,j} A_i(\lambda_{exc})\, F_j(\lambda_{em})[2 - cos^2\, \theta_{ij}] \qquad (5b)$$

and $A_i(\lambda_{exc})$ measures the absorbance from the ground to the *i*th excited state (*i* runs on all exact nonadiabatic excited states) at the excitation wavelength λ_{exc}; $F_j(\lambda_{em})$ measures the fluorescence intensity from the emitting state toward the *j*th state (*j* runs on all exact nonadiabatic states with lower energy than the emitting state) at the wavelength λ_{em}; θ_{ij} is the angle between the transition dipole moments relevant to the absorption process (from the ground to the *i*th state) and the fluorescence process (from the fluorescent state to the *j*th state). In the calculation of fluorescence emission anisotropy λ_{exc} is kept fixed while λ_{em} is varied, and the opposite is done for the calculation of fluorescence excitation anisotropy spectra.

To clarify the picture, we make reference to Figure 6, where the relevant absorption processes are marked by blue arrows and the fluorescence process is marked by a red arrow. Indeed, this picture

only shows electronic states, while the states entering eqs 5a and 5b are vibronic eigenstates obtained from the diagonalization of the nonadiabatic Hamiltonian. Moreover, in the purely electronic model described in Figure 6, the states E_1 and E_2 are degenerate for $V = 0$, while in the complete model slow (solvation and configurational) coordinates break the symmetry of the system, removing the E_1–E_2 degeneracy whenever $F_x \neq F_y$ or $R_1 \neq R_2$, quite irrespective of V. Absorption spectra, and hence the absorbance entering eqs 5a and 5b, are calculated accounting for the transitions from the ground state toward the two first electronic excited states (E_1 and E_2), characterized by mutually orthogonal transition dipole moments (of course the calculation actually involves relevant vibronic states). Energy transfer enters the model imposing that after excitation the system relaxes downward toward the lowest-energy electronic excited state (the fluorescent state), as sketched in Figure 6. To be more precise, since vibrational energies are much larger than thermal energies, the fluorescent state corresponds to the lowest vibronic eigenstate relevant to the lowest electronic excited state. The fluorescence intensity in eqs 5a and 5b is therefore calculated starting from the fluorescent state toward all vibronic states associated with the electronic ground state. Indeed, for very small V (as relevant to **S1**) the two lowest electronic excited states are almost degenerate when $F_x \cong F_y$ and $R_1 \cong R_2$, and we explicitly account for the relative populations of the two states, as governed by the Boltzmann law. However, this only marginally contributes to overall spectra.

Electronic and vibrational energies are in general much larger than thermal energies, and Boltzmann averages are therefore irrelevant (apart from the special case when $V \cong 0$, $F_x \cong F_y$, and $R_1 \cong R_2$). However, the energy of the vibronic states shows a continuous dependence on slow coordinates (treated as classical variables in our work). Thermal population of this continuum leads to inhomogeneous broadening effects in calculated spectra. The delicate point in the calculation is the definition of Boltzmann averages for $I_\parallel$ and $I_\perp$ over the points of the (hyper)space described by the slow coordinates, properly accounting for the relaxation of the internal conformational coordinate(s) (R for the chromophore, R_1 and R_2 for the spiro dimer) while maintaining the distribution of the relevant component(s) of the solvent reaction field (F for the chromophore, F_x and F_y for the spiro dimer) frozen at the equilibrium for the ground state. With reference to the isolated chromophore, the $I_\parallel$ and $I_\perp$ values calculated according to eqs 5a and 5b on each point of the (F,R) grid must be weighted by the probability:

$$P(F,R) = \tilde{p}_{gs}(F)\frac{p_{gs}(F,R)\,p_{fs}(F,R)}{\sum_R p_{gs}(F,R)\sum_R p_{fs}(F,R)} \qquad (6)$$

Where

$$p_{gs}(F,R) = \frac{\exp[-E_{gs}(F,R)/kT]}{\sum_F \exp[-E_{gs}(F,R)/kT]} \qquad (7)$$

is the Boltzmann population of the (F,R) point of the grid for the ground state. The corresponding probability for the fluorescent state, $p_{fs}(F,R)$, is given by a similar equation with the (F- and R-dependent) ground state energy, $E_{gs}(F,R)$, substituted by the energy of the fluorescent state, $E_{fs}(F,R)$. Finally

$$\tilde{p}_{gs}(F) = \frac{\sum_{R} p_{gs}(F,R)}{\sum_{R,F} p_{gs}(F,R)} \qquad (8)$$

Similar equations hold for spiro dimers, with the sums on F and R extended to the pairs of F_x and F_y and R_1 and R_2 variables. Once the averaged $I_{\parallel}$ and $I_{\perp}$ are obtained, the anisotropy is calculated according to eq 1.

Fluorescence emission and excitation spectra are a byproduct of the anisotropy calculation: fluorescence spectra are obtained plotting $I_{\parallel} + 2I_{\perp}$ vs λ_{em} for fixed λ_{exc}; fluorescence excitation spectra are obtained plotting the same quantity at fixed λ_{em} and varying λ_{exc}.

Figure 8 shows calculated spectra of the **P2**/**S2** pair in frozen decalin, adopting the same parameters extracted from the analysis of room-temperature spectra (cf. Table 2) and setting the temperature to 200 K. Analogous results are obtained for the **P1**/**S1** pair and are reported as Supporting Information. **P2** is modeled as a linear molecule with collinear absorption and fluorescence transition dipole moments, leading to r = 0.4. The observed r > 0.3 suggests a marginal noncollinearity of the two transition dipole moments in the actual molecular structure. For spiro dimers, in good agreement with experimental data, a flat anisotropy excitation spectrum with $r \sim$ 0.1 is calculated within the excitation band, with a gradual increase only in the red edge of the spectrum. Accordingly, calculated emission anisotropy spectra are barely affected by the excitation wavelength. Calculated emission bands agree well with experimental data, even if calculated fluorescence spectra are more resolved than experimental spectra. We underline that, to minimize the number of adjustable parameters, we keep all model parameters fixed to the room-temperature estimate. Of course, better fits could be obtained accounting for variations of the vibrational frequency and/or relaxation energy with temperature.

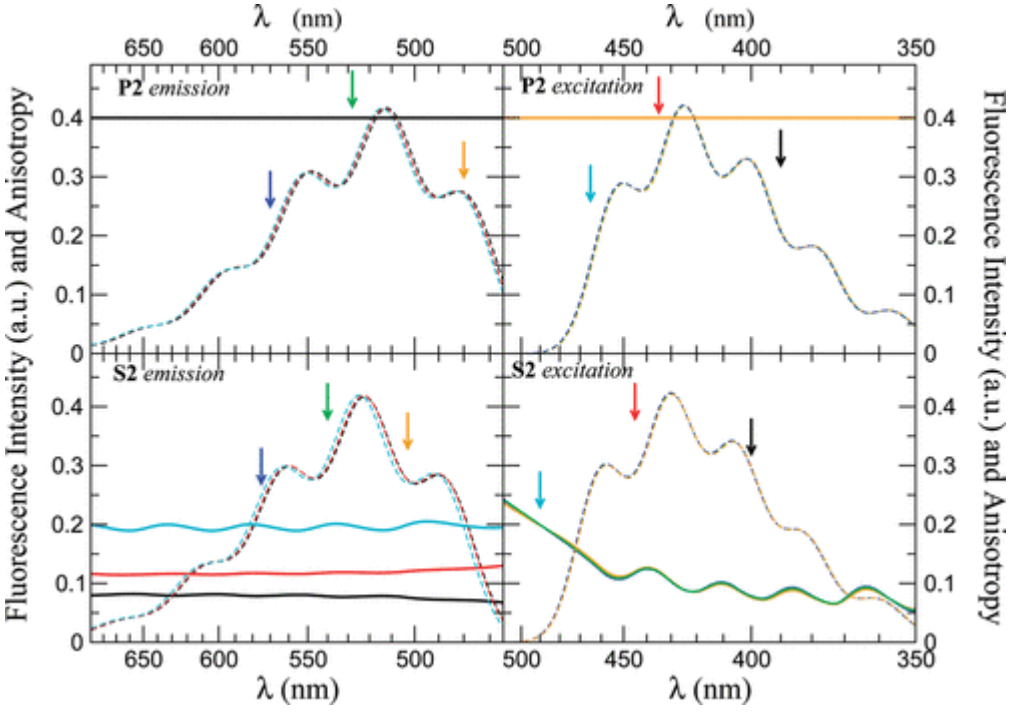

Figure 8. Calculated fluorescence and fluorescence anisotropy spectra of **P2** (top panels) and **S2** (bottom panels) in glassy decalin matrixes, adopting model parameters in Table 2. The same symbols and color code are adopted as in Figure 3.

Figure 9 shows the spectra calculated for **P2** and **S2** in glassy 2-MeTHF matrixes (similar results for **P1** and **S1** can be found as Supporting Information). The calculations are run imposing the glass transition temperature of 2-MeTHF (90 K). In this case, to better reproduce the spectral position, we allowed for a small decrease of η with respect to the room-temperature value (cf. Table 2). This is consistent with the increase of the 2-MeTHF refractive index with decreasing temperature,(21) which stabilizes the zwitterionic state.(22, 26) As expected for a polar and almost linear dye, and in agreement with experimental results, anisotropy spectra of **P2** are flat with a large *r*. Calculated excitation anisotropy spectra of **S2** show instead a well-pronounced variation *within* the excitation band: *r* is low in the blue edge of the excitation band and increases rapidly toward the limiting 0.4 value in the red side of the excitation band. Accordingly, emission anisotropy spectra show an important dependence on the excitation wavelength. In close agreement with experimental data, calculated spectra in the frozen polar solvent show a qualitatively different behavior from spectra calculated in the nonpolar frozen solvent (decalin): in the nonpolar solvent in fact the anisotropy increases only in the very far red edge of the excitation band, while in the polar solvent the increase is much steeper and is observed *well inside* the excitation band. This behavior is related to the solvent polarity, and in fact it is observed also for $V = 0$ (cf. results for **S1** in the Supporting Information).

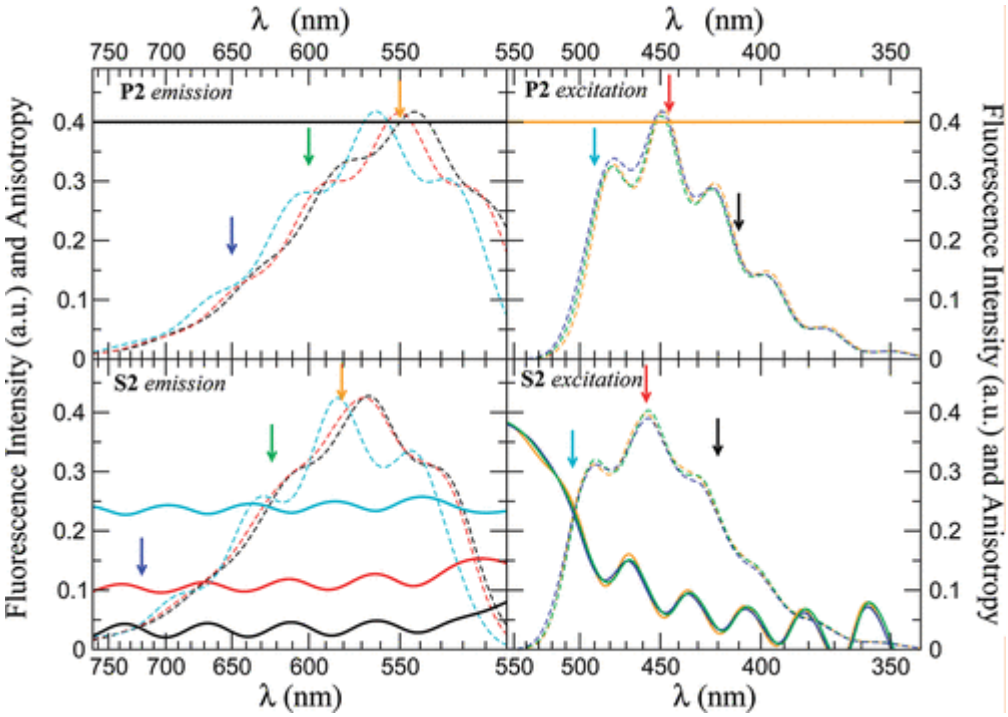

Figure 9. Calculated fluorescence and fluorescence anisotropy spectra of **P2** (top panels) and **S2** (bottom panels) in glassy 2-MeTHF matrixes, adopting model parameters in Table 2. The same symbols and color code are adopted as in Figure 4.

The calculated anisotropy for **S2** (Figures 8 and 9) shows an oscillating behavior, related to the different polarizations of vibronic transitions. These oscillations are most probably smoothed in experimental systems due to the presence of more than one coupled vibrational mode, and in any case their experimental observation would be hindered by noise.

Discussion and Conclusions

In this paper we presented a joint experimental and theoretical work on optical spectra of donor–acceptor substituted fluorene chromophores, **P1** and **P2**, and the corresponding spiro dimers, **S1** and **S2**, focusing attention on fluorescence and fluorescence anisotropy spectra. A bottom-up modeling approach is adopted to rationalize the dimer behavior based on essential-state models. Specifically, the strongly solvatochromic absorption and fluorescence spectra of chromophores **P1** and **P2** are quantitatively reproduced using the standard two-state model for donor–acceptor polar dyes(23, 25-27) extended to account for the presence of a slow internal (conformational) degree of freedom,(22, 23) as needed to reproduce the observation of broad absorption spectra and of sizable Stokes shifts in nonpolar solvents. In the spirit of the bottom-up approach,(29-33) the information extracted from the analysis of solution spectra of **P1** and **P2** is used to build models for the spiro dimers **S1** and **S2**: the spectra of the dimers are quantitatively reproduced using the same model parameters adopted for the isolated chromophores and adjusting a single additional parameter, *V*, that describes the effective interaction between the two moieties. Indeed, the interchromophore interaction is negligible in **S1** ($V = 0$) and fairly small in **S2** ($V = -0.4$ eV). *V* formally enters the model as an electrostatic interaction; however positive *V* values (repulsive electrostatic interchromophore interactions) are expected in the spiro geometry. The negative *V* value extracted for **S2** from the analysis of experimental data therefore represents an effective interaction accounting not only for electrostatic forces but also for other effects, including, e.g., spiroconjugation.

The success of essential-state models in the calculation of absorption and fluorescence spectra of polar chromophores and of their spiro dimers invites the investigation of other spectroscopic data. Fluorescence anisotropy is particularly interesting for spiro dimers because it offers detailed information about the relative orientation of absorption and fluorescence dipole moments, and then gives hints about the transfer of excitation energy between the two chromophores.(24) Indeed, absorption and fluorescence spectra of spiro dimers are very similar to those of corresponding isolated chromophores, pointing to weak intermolecular interactions. However, anisotropy spectra of spiro dimers are qualitatively different from those of the corresponding fluorene-substituted chromophores, unambiguously demonstrating that intramolecular energy transfer occurs after photoexcitation. Therefore, while interchromophore interactions are weak and only marginally affect absorption and fluorescence spectra, they are large enough to effectively induce energy transfer between excited states. Indeed, to appreciably alter absorption or fluorescence spectra, sizable interaction energies are needed compared to vertical energy gaps between excited states. By contrast, energy transfer involves relaxed states and may occur in the proximity of surface crossing, where even tiny interactions play a significant role.(34) The reduction of the fluorescence quantum yield in spirodimers (cf. Table 1) confirms the importance of interchromophore interactions in the photophysics of these systems. However, while essential-state models can be quantitative in the calculation of absorption, fluorescence, and anisotropy spectra, they can hardly address quantum yields, where a major role is played by the competition between radiative and nonradiative decay channels.

Spectra of **S1** and **S2** in glassy solvents show an interesting and strongly solvent-dependent behavior. In nonpolar rigid matrixes, such as decalin, emission and excitation spectra of spiro dimers are independent of excitation and emission wavelengths, respectively. Fluorescence excitation anisotropy is basically flat within the excitation band and increases just at the far red edge of the

band. By contrast, in the polar rigid matrix (2-MeTHF), fluorescence excitation anisotropy shows an important increase already *within* the excitation band, and excitation (emission) spectra red-shift as emission (excitation) wavelengths are moved toward the red. The anomalous spectroscopic behavior observed in rigid polar matrixes goes under the general name of "red-edge effect". The concept of red-edge effect was introduced in the 1970s with reference to the dependence of emission spectra collected in glassy matrixes on the excitation frequency.(35) The phenomenon was ascribed to inhomogeneous broadening in frozen polar solvents associated with the thermal distribution of the orientations of the polar solvent molecules around the solute. In a rigid matrix the excitation at a specific wavelength results in the photoselection of a subset of molecules out of the distribution:(35) since the solvent relaxation is hindered (in a rigid matrix only internal molecular modes can relax), the emitting state is specific of photoselected molecules, causing a dependence of spectral properties upon excitation wavelengths. Moreover, in inhomogeneously broadened samples, excitation in the red edge of the absorption band photoselects the species in the sample that absorb at the lowest energies: in multichromophoric systems, where energy transfer becomes relevant, this photoselection will hinder energy transfer (homotransfer) to lower-lying states, explaining the observation of anisotropies rising toward the limiting 0.4 value for excitation in the red edge of the absorption band.(36, 37)

The basic physics underlying red-edge effects is well understood, but only recently quantitative models for anisotropy spectra in polar rigid matrixes have been proposed and applied to octupolar charge-transfer chromophores.(24) In these highly symmetric chromophores, the two lowest excitations are degenerate with mutually orthogonal transition dipole moments. Red-edge effects are related to, and have been quantitatively modeled in terms of, the distribution of reaction fields in polar solvents.(24) Molecules experiencing a finite reaction field in fact experience a reduced symmetry leading to the splitting of the two excited states. Upon excitation in the red edge of the absorption band, only the lower-energy excited state is accessed and this state cannot down-transfer its energy, so $r \rightarrow 0.4$. Our spiro dimers are qualitatively different from octupolar chromophores and show in general a distinctively different spectroscopic behavior. However, a similarity in the two families of compounds is recognized in the presence of two degenerate or almost degenerate fluorescent states, with mutually orthogonal transition dipole moments. In both families of compounds a finite reaction field splits the two states: red-edge effects observed for spiro dimers in glassy polar solvents have exactly the same physical origin as red-edge effects discussed in ref 24 for octupolar chromophores.

According to the previous discussion, and as confirmed by essential-state models, the origin of red-edge effects in the spectra of **S1**/**S2** collected in 2-MeTHF is ascribed to exciton splitting promoted by finite reaction fields in polar solvent. This is supported by spectra collected in the nonpolar solvent, decalin, which show only a very weak red-edge effect just in the far red edge of the excitation band. This behavior is accounted for in our calculation assigning decalin a very small relaxation energy ε_{or} = 0.02 eV. The low-frequency conformational degree of freedom never plays an active role in the red-edge effect, because the associated coordinate is not frozen and relaxes after photoexcitation.

Overall, essential-state models lead to a detailed and satisfactory description of optical spectra of polar chromophores, **P1** and **P2**, and of their spiro dimers, **S1** and **S2**, based on a minimal set of

model parameters, rationalizing many subtle effects related to polar solvation. Essential-state models are very robust and were successfully applied to several systems. In particular, once parametrized against linear spectra, essential-state models reliably describe nonlinear optical spectra.(28, 33, 38, 39) Second harmonic generation was previously investigated for the systems discussed in this work via the EFISH technique.(19) In Table 3 we report the permanent dipole moment and the first hyperpolarizability calculated according to our model (details about the calculation of hyperpolarizability within essential-state models can be found in ref 28). Both the dipole moments and the hyperpolarizabilities calculated for the spiro dimers are about a factor √2 larger than for the relevant monomeric chromophores, corresponding to the vectorial sum of the contributions from the two (mutually orthogonal) chromophores. This result confirms once more the additivity of the properties of spiro dimers, as expected in view of the very small interchromophore interactions. Essential-state hyperpolarizabilities are in perfect agreement with time-dependent DFT results,(19) but contrast experimental data.(19)

Table 3. Permanent Dipole Moments and First Hyperpolarizabilities Calculated with Model Parameters in Table 2 **2** for ε_{or} = 0.7 (Corresponding to Chloroform)

	μ (D)	β^0_{EFISH}[a] (10^{-30} esu)	β_{EFISH}[b] (10^{-30} esu)
P1	2.38	42	44
S1	3.36	59	62
P2	2.92	125	132
S2	4.29	196	208

[a] Static first hyperpolarizability.
[b] First hyperpolarizability calculated at 1907 nm.

In conclusion, we presented an extensive spectroscopic study of two substituted fluorene dyes, **P1** and **P2**, and of the related spiro dimers, **S1** and **S2**, in both liquid and glassy solvents. Essential-state models have been developed to accurately reproduce linear absorption and fluorescence spectra and their complex dependence on the solvent polarity. Of particular interest in this context is the possibility offered by the models to quantitatively calculate fluorescence and excitation anisotropy spectra in rigid matrixes. Impressive red-edge effects observed for spiro dimers in glassy polar solvents are accurately reproduced and understood, clearly demonstrating that while interchromophore interactions are too small in spiro dimers to significantly alter absorption and fluorescence spectra, they effectively induce energy transfer between the two chromophores, in line with the recent observation of complex photophysical behavior of spiro-linked materials.(16-18)

Supporting Information

Experimental and calculated fluorescence and fluorescence anisotropy spectra of **P1** and **S1** in glassy solutions of decalin and 2-MeTHF. This material is available free of charge via the Internet at http://pubs.acs.org.

References

’REFERENCES

(1) (a) Bredas, J. L.; Cornil, K; Meyers, F.; Beljonne, D. In Handbook of Conducting Polymers; Skotheim, T. A., Elsenbaumer, R. L., Reynolds, J. R., Eds.; Marcel Dekker: New York, 1998; pp 1-26. (b) Soos, Z. G.; Painelli, A.; Girlando, A.; Mukhopadhyay, D. In Handbook of Conducting Polymers; Skotheim, T. A., Elsenbaumer, R. L., Reynolds, J. R., Eds.; Marcel Dekker: New York, 1998; pp 165-196. (c) Metzger, R. M. J. Mater. Chem. 2008, 18, 4364–4396. (d) Cicoira, F.; Santato, C. Adv. Mater. 2007, 17, 3421–3434. (e) Vogel, E. M. Nat. Nanotechnol. 2007, 2, 25–32. (f) Liu, J.; Chen, L.; Shao, S.; Xie, Z.; Cheng, Y.; Geng, Y.; Wang, L.; Jing, X.; Wang, F. Adv. Mater. 2007, 19, 4224–4228. (g) Clarke, T. M.; Durrant, J. R. Chem. Rev. 2010, 110, 6736–6767.

(2) (a) Marder, S. R.; Kippelen, B.; Jen, A. K.-Y.; Peyghambarian, N. Nature 1997, 388, 845–851. (b) Marder, S. R.; Torruellas, W. E.; Blanchard-Desce, M.; Ricci, V.; Stegeman, G. I.; Gilmour, S.; Bredas, J.-L.; Li, J.; Bublitz, G. U.; Boxer, S. G. Science 1997, 276, 1233–1236. (c) Albota, M.; Beljonne, D.; Bredas, J.-L.; Ehrlich, J. E.; Fu, J.-Y.; Heikal, A. A.; Hess, S. E.; Kogej, T.; Levin, M. D.; Marder, S. R.; et al. Science 1998, 281, 1653–1656. (d) Mongin, O.; Porres, L.; Charlot, M.; Katan, C.; Blanchard-Desce,M.Chem.;Eur. J.2007, 13, 1481–1498. (e) Elangovan, A.; Sullivan, P. A.; Olbricht, B. C.; Bale, D. H.; Ewy, T. R.; Isborn, C. M.; Eichinger, B. E.; Robinson, B. H.; Reid, P. J.; Li, X.; et al. J. Am. Chem. Soc. 2008, 130, 10565–10575.

(3) (a) Bredas, J. L.; Beljonne, D.; Coropceanu, V.; Cornil, J. Chem. Rev. 2004, 104, 4971–5003. (b) Liao, Y.-L.; Hung, W.-Y.; Hou, T.-H.; Lin, C.-Y.; Wong, K.-T. Chem. Mater. 2007, 19, 6350–6357. (c) Husta, H.; Risko, C.; Wang, Z.; Huang, H.; Deliomeroglu, M. K.; Zhukhovitskiy, A.; Facchetti, A.; Marks, T. J. J. Am. Chem. Soc. 2009, 131, 5586–5608. (d) Viani, L.; Olivier, Y.; Athanasopoulos, S.; da Silva Filho, D. A.; Hulliger, J.; Bredas, J.-L.; Gierschner, J.; Cornil, J. ChemPhysChem 2010, 11, 1062–1068.

(4) (a) Ashwell, G. J.; Leeson, P.; Bahra, G. S.; Brown, C. R. J. Opt. Soc. Am. B 1998, 15, 484–488. (b) Drobizhev, M.; Stepanenko, Y.; Dzenis, Y.; Karotki, A.; Rebane, A.; Taylor, P. N.; Anderson, H. L. J. Am. Chem. Soc. 2004, 126, 15352. (c) Collini, E.; Ferrante, C.; Bozio, R. J. Phys. Chem. B 2005, 109, 2. (d) Belfield, K. D.; Bondar, M. V.; Hernandez, F. E.; Przhonska, O. V.; Yao, S. Chem. Phys. 2006, 320, 118. (e) Liu, X.; Xu, J.; Li, Y.; Li, Y. Acc. Chem. Res. 2010, 43, 1496–1506.

(5) (a) Terenziani, F.; Painelli, A. Phys. Rev. B 2003, 68, 165405. (b) Painelli, A.; Terenziani, F. J. Am. Chem. Soc. 2003, 125, 5624–5625. (c) Painelli, A.; Terenziani, F. In Non-Linear Optical Properties of Matter; Papadopoulos, M. G., et al. , Eds.; Springer: New York, 2006; pp 251-282. (d) Terenziani, F.; D’Avino, G.; Painelli, A. ChemPhysChem 2007, 8, 2433–2444.

(6) Saragi, T. P. I.; Spehr, T.; Siebert, A.; Fuhrmann-Lieker, T.; Salbeck, J. Chem. Rev. 2007, 107, 1011–1065.

(7) Johansson, N.; dos Santos, D. A.; Guo, S.; Cornil, J.; Fahlman, M.; Salbeck, J.; Schenk, H.; Arwin, H.; Bredas, J. L.; Salanek, W. R. J. Chem. Phys. 1997, 107, 2542–2549.

(8) Simmons, H. E.; Fukunaga, T. J. Am. Chem. Soc. 1967, 89, 5208–5215.

(9) Hoffmann, R.; Imamura, A.; Zeiss, G. D. J. Am. Chem. Soc. 1967, 89, 5215–5220.

(10) Gordon, M. D.; Fukunaga, T.; Simmons, H. E. J. Am. Chem. Soc. 1976, 98, 8401–8407.

(11) Chiang, C.-L.; Wu, M.-F.; Dai, D.-C.; Wen, Y. S.; Wang, J.-K.; Chen, C.-T. Adv. Funct. Mater. 2005, 15, 231–238.

(12) Pudzich, R.; Salbeck, J. Synth. Met. 2003, 138, 21–31.

(13) Chiang, C.-L.; Shu, C.-F.; Chen, C.-T. Org. Lett. 2005, 7, 3717–3720.

(14) Wu, C. C.; Liu, W. G.; Hung, W. Y. Appl. Phys. Lett. 2005, 87, 052103.

(15) Laquai, F.; Wegner, G.; Im, C. J. Appl. Phys. 2006, 99, 023712.

(16) Hintschich, S. I.; Rothe, C.; King, S. M.; Clark, S. J.; Monkman, A. P. J. Phys. Chem. B 2008, 112, 16300–16306.

(17) Milota, F.; Warmuth, Ch.; Tortschanoff, A.; Sperling, J.; Fuhrmann, T.; Salbeck, J.; Kauffmann, H. F. Synth. Met. 2001, 121,1497–1498.

(18) Brendel, C. M.; Dias, F. B.; Saragi, T. P. I.; Monkman, A. P.; Salbeck, J. Phys. Status Solidi A 2009, 206, 2715–2722.

(19) Rizzo, F.; Cavazzini, M.; Righetto, S.; De Angelis, F.; Fantacci, S.; Quici, S. Eur. J. Org. Chem. 2010, 4004–4016.

(20) Lakowicz, J. R. Principles of Fluorescence Spectroscopy; Kluwer Academic/Plenum Publishers: New York, 1999.

(21) Nicholls, D.; Sutphen, C.; Szwarc, M. J. Phys. Chem. 1968, 72, 1021–1027. Pineiro, A.; Brocos, P.; Amigo, A.; Pintos, M.; Bravo, R. J. Solution Chem. 2002, 31, 369–380.

(22) Sissa, C.; Terenziani, F.; Painelli, A.; Abbotto, A.; Bellotto, L.; Marinzi, C.; Garbin, E.; Ferrante, C.; Bozio, R. J. Phys. Chem. B 2010, 114, 882–893.

(23) Painelli, A.; Terenziani, F. J. Phys. Chem. A 2000, 104, 11041–11048. Terenziani, F.; Painelli, A.; Comoretto, D. J. Phys. Chem. A 2000, 104, 11049–11054.

(24) Sissa, C.; Painelli, A.; Blanchard-Desce, M.; Terenziani, F. J. Phys. Chem B 2011, 115, 7009–7020.

(25) Painelli, A. Chem. Phys. Lett. 1998, 285, 352–358. Painelli, A.; Terenziani, F. Chem. Phys. Lett. 1999, 312, 211–220.

(26) Painelli, A. Chem. Phys. 1999, 245, 185–197.

(27) Boldrini, B.; Cavalli, E.; Painelli, A.; Terenziani, F. J. Phys. Chem. A 2002, 106, 6286–6294.

(28) Grisanti, L.; Sissa, C.; Terenziani, F.; Painelli, A.; Roberto, D.; Tessore, F.; Ugo, R.; Quici, S.; Fortunati, I.; Garbin, E.; Ferrante, C.; Bozio, R. Phys. Chem. Chem. Phys. 2009, 11, 9450–9457.

(29) D'Avino, G.; Terenziani, F.; Painelli, A. J. Phys. Chem. B 2006, 110, 25590–25592.

(30) Painelli, A.; Terenziani, F.; Angiolini, L.; Benelli, T.; Giorgini, L. Chem.;Eur. J. 2005, 11, 6053–6063.

(31) Datta, A.; Terenziani, F.; Painelli, A. ChemPhysChem 2006, 7, 2168–2174.

(32) D'Avino, G.; Grisanti, L.; Guasch, J.; Ratera, I.; Veciana, J.; Painelli, A. J. Am. Chem. Soc. 2008, 130, 12064–12072.

(33) Todescato, F.; Fortunati, I.; Carlotto, S.; Ferrante, C.; Grisanti, L.; Sissa, C.; Painelli, A.; Colombo, A.; Dragonetti, C.; Roberto, D. Phys. Chem. Chem. Phys. 2011, 13, 11099–11109.

(34) Sissa, C.; Manna, A. K.; Terenziani, F.; Painelli, A.; Pati, S. K. Phys. Chem. Chem. Phys. 2011, 13, 12734–12744.

(35) Demchenko, A. P. Luminescence 2002, 17, 19–42.

(36) Berberan-Santos, M. N.; Pouget, J.; Valeur, B.; Canceill, J.; Jullien, L.; Lehn, J.-M. J. Phys. Chem. 1993, 97, 11376–11379.

(37) Weber, G.; Shinitzky, M. Proc. Natl. Acad. Sci. U.S.A. 1970, 65, 823–830.

(38) Campo, J.; Painelli, A.; Terenziani, F.; Van Regemorter, T.; Beljonne, D.; Goovaerts, E.; Wenseleers, W. J. Am. Chem. Soc. 2010, 132, 16467–16478.

(39) Terenziani, F.; Przhonska, O. V.; Webster, S.; Padilha, L. A.; Slominsky, Y. L.; Davydenko, I. G.; Gerasov, A. O.; Kovtun, Y. P.; Shandura, M. P.; Kachkovski, A. D.; et al. J. Phys. Chem. Lett. 2010, 1, 1800–1804.